The Synergistic Effect of Cold Atmospheric Plasma Mediated Gold Nanoparticles Conjugated with Indocyanine Green as An Innovative Approach to Cooperation with Radiotherapy

Sara Momeni, M.Sc.[1], Ahmad Shanei, Ph.D.[1*], Ameneh Sazgarnia, Ph.D.[2*], Neda Attaran, Ph.D.[3],

Seyed Amir Aledavood, M.D.[4]

1. Department of Medical Physics, School of Medicine, Isfahan University of Medical Sciences, Isfahan, Iran
2. Medical Physics Research Center, Mashhad University of Medical Sciences, Mashhad, Iran
3. Department of Medical Nanotechnology, Science and Research Branch, Islamic Azad University, Tehran, Iran
4. Cancer Research Center, Faculty of Medicine, Mashhad University of Medical Sciences, Mashhad, Iran

*Corresponding Addresses: P.O.Box: 8174673461, Department of Medical Physics, School of Medicine, Isfahan University of Medical Sciences, Isfahan, Iran
P.O.Box: 9177948564, Medical Physics Research Center, Mashhad University of Medical Sciences, Mashhad, Iran
Emails: Shanei@med.mui.ac.ir, sazgarniaa@mums.ac.ir*

Abstract
Objective: The multimodality treatment of cancer provides a secure and effective approach to improve the outcome of treatments. Cold atmosheric plasma (CAP) has got attention because of selectively target and kills cancer cells. Likewise, gold nanoparticles (GNP) have been introduced as a radiosensitizer and drug delivery with high efficacy and low toxicity in cancer treatment. Conjugating GNP with indocyanine green (ICG) can develop a multifunctional drug to enhance radio and photosensitivity. The purpose of this study is to evaluate the anticancer effects of GNP@ICG in radiotherapy (RT) and CAP on DFW melanoma cancer and HFF fibroblast normal cell lines.

Materials and Methods: In this experimental study, the cells were irradiated to RT and CAP, alone and in combination with or without GNP@ICG at various time sequences between RT and CAP. Apoptosis Annexin V/PI, MTT, and colony formation assays evaluated the therapeutic effect. Finally, the index of synergism was calculated to compare the results.

Results: Most crucially, the cell viability assay showed that RT was less toxic to tumors and normal cells, but CAP showed a significant anti-tumor effect on melanoma cells with selective toxicity. In addition, cold plasma sensitized melanoma cells to radiotherapy so increasing treatment efficiency. This effect is enhanced with GNP@ICG. In comparison to RT alone, the data showed that combination treatment greatly decreased monolayer cell colonization and boosted apoptotic induction.

Conclusion: The results provide new insights into the development of better approaches in radiotherapy of melanoma cells assisted plasma and nanomedicine.

Keywords: Apoptosis, Cold Plasma, Indocyanine Green, Melanoma, Radiation Therapy

Introduction

Cancer is a significant burden of disease on a global scale. Melanoma, a malignant tumor originating from melanocytes, is a rare disease and the most deadly type of skin cancers (1). Despite the fact that surgery is the main treatment option, radiotherapy (RT) is sometimes required for tumor size reduction, adjuvant therapy postoperatively, and lymph node or brain metastasis. Thus, a great number of studies have been conducted in an attempt to increase the sensitivity of radiotherapy-resistant cells and reduce side effects (2).

Photodynamic therapy (PDT) is a new therapeutic method with Food and Drug Administration (FDA) approval used to treat superficial tumors, such as skin cancer (3, 4). PDT uses a particular drug called photosensitizer along with light to cause oxygen-dependent destruction of cancer cells. Although they are not individually toxic, photochemical reactions produce highly reactive products called singlet oxygen ($^1O_2$),

which can rapidly cause cell death via apoptosis and necrosis (5). However, PDT as an adjunct therapy offers several benefits, there are some limitations about PDT such as hypoxia induction due to oxygen consumption and vascular damage, not being tumor-specific method and etc. (6, 7).

The ionized plasma known as cold atmospheric plasma (CAP) may be employed as a new light source for PDT. CAP is an ionized gas contains electrons, ions, free radicals, reactive oxygen (ROS) and nitrogen species (RNS), and UV photons that exists at low temperatures. At atmospheric pressure, plasma is created by using a high voltage electric field (8). Because CAP is a potent generator of ROS, it may help to reduce some problems related to PDT and increase therapeutic effectiveness (9). In general, plasma is classified into two types: thermal plasma and non-thermal or cold plasma. In the past, only the thermal properties of plasma had biomedical uses in ablation, tissue cutting, and blood coagulation.

Recent research into the medical applications of CAP has revealed new areas of medical research. Some of the medical applications of CAP include wound healing (10), sterilization of medical devices , and induction of blood clotting during surgery (11). The anti-cancer effects of CAP were studied in various types of cancer, *in vitro* (12) and *in vivo* (13). The most noticeable feature of CAP is the ability to kill cancer cells selectively and protect healthy cells (14). Although the mechanism of contact between plasma and cell is not fully known, ROS seems to play a critical role in this process (15). More ROS diffuses into tumor cells because they have more AQPs (an aquatic channel that increases ROS diffusion through transmembrane) and more cholesterol in their cellular membrane than normal cells, resulting in higher oxidative balance disruption (16). Normal cells, on the other hand, are better at dealing with this disruption than tumor cells (17). The studies proposed various mechanisms of CAP effects containing oxidative stress, ROS generation and subsequently DNA double strands break (DSB), cell cycle arrest, activation of *p53* gene, and activation of p21 CKS inhibitor, necrosis, cell detachment and apoptosis via plasma-generated ROS (18-20).

Cancer treatment with integration of CAP and nanoparticles has shown to be lucrative. Gold nanoparticles (GNP) exhibit unique qualities among nanoparticles, including low toxicity, tumor-specific drug transporters, radiosensitizers, and changeable absorption peak from ultra-violet to infrared depending on particle shape and size (21). The benefits of cancer treatment with CAP and GNP are most likely ascribable to their more selectivity, rise in nanoparticles uptake, and better treatment efficiency (22, 23). Indocyanine green (ICG) is a low toxic amphilic dye with Food and Drug Administration (FDA) approval used for cancerous photothermal and PDT (24). ICG shows high absorbance in the treatment window (650-850 nm) where maximum light transmission to the tissue occurs that is not absorbed by the melanin of the skin or melanoma cells. It can be used as a photosensitizer along with GNP to evaluate the photodynamic effects evoked by CAP.

The impacts of combined radiation therapy (RT) with CAP were reported in some research. However, no study has been performed to investigate the composition of CAP as a pre-treatment of RT in the presence of a photo-radio sensitizer, with the hypothesis that it can amplify the radiation as well as photodynamic effects produced by the plasma. Besides, the point that is less considered in combination therapies is the sequence of treatments and its effect on the final result. It has generally been proven that different treatments can stop the cell cycle. Therefore, applying a treatment that stops the cells in the radiation-sensitive phase, followed by RT, increases the effectiveness of the treatment.

Hence, we evaluated new technique for treating melanoma cells *in vitro*. The radiosensitizing effect mediated by plasma-induced PDT in the presence of GNP@ICG on the DFW human melanoma cell line and HFF normal fibroblast cell line is the main aim of this study. In this case, GNP@ICG NPs were initially synthesized and their photophysical characteristics studied. Second, the effectiveness of GNP@ICG in PDT caused by CAP treatment on cancer and normal cells, as well as its selectivity, were assessed. Third, the radio-sensitization impact of GNP@ICG was investigated at various dosages. Fourth, treatments were carried out at 0 and 24 hours intervals to identify the optimal time between CAP and RT. Finally, the mechanism of death in combination therapy and each treatment alone was evaluated by flow cytometry to diagnose apoptosis.

Materials and Methods

Ethics approval for the current experimental study was given by the Ethics Committee at Isfahan University of Medical Sciences under a project number of IR.MUI. MED.REC.1399.947. Gold (III) chloride hydrate (99.995 %) was acquired by Alfa Asear (254169, USA). Fetal bovine serum (FBS) was acquired by Gibco (F7524, USA). ICG (228869) and dimethyl sulfoxide (DMSO, D8418) were acquired by Merck (Germany). Trisodium citrate dehydrate (6132-04-3), Roswell Park Memorial Institute (RPMI-1640, 51800-035) cell culture medium, Dulbeccos Modified Eagles Medium (DMEM, D6429), penicillin-streptomycin (P4333), trypsin-ethylene diamine tetra acetic acid (EDTA, 60-00-4), and 3–(4,5dimethylthiazol-2-yl)-2,5-diphenyltetrazolium bromide (MTT,TOX1) were acquired by Sigma-Aldrich Company (St. Louis, MO, USA). Apoptosis Detection Kit [Annexin V labeled with FITC/Propidium Iodide (PI)] was purchased from BD Biosciences (AB_2869082, USA).

Synthesis and physical characterization

GNP and GNP@ICG synthesis

GNP@ICG nanoparticles were synthesized in a two-step process. First step: GNP were synthesized as stated in Anshup et al. (25). All glassware was scrubbed with a 3:1 solution of HCl and HNO_3, after that washed with distilled water and drained. A solution containing HAuCl4 (5 ml, 0.2% w/w) and deionized water (90 ml) was refluxed under constant and vigorous stirring. When the solution reached boiling point, sodium citrate trihydrate (5 ml, 1% w/w) was rapidly infused into the HAuCl4 solution. The molar ratio of sodium citrate trihydrate to HAuCl4 was a major controlling factor in achieving the desired particle size. After changing the color from pale yellow to red, the solution was remained for 15 minutes. GNP produced were purified by centrifugation and repeated precipitation from distilled water. Second step: To conjugate ICG on the GNP surface, we added an aqueous solution of ICG (10 ml, 80 mg/L) to the GNP preparation solution (10 ml, 100 mg/L) and at room temperature stirred for 3 hours. After the completion time, the particles were centrifuged and precipitated twice from distilled water to give purified GNP@ICG nanoparticles.

Characterization of GNP and GNP@ICG

Particle size, size distribution, and polydispersity index (PDI) for GNP and GNP@ICG were obtained using the Malvern Zetasizer (Zetasizer, Malvern Ins., USA). To assess the stability of GNP and GNP@ICG, we performed dynamic light scattering (DLS) analysis of NPs at different time points. For this purpose, 125 µl of GNP and 90 µl of GNP@ICG were added to 875 and 910 µl of 10% fetal bovine serum (FBS) supplemented culture medium, respectively and DLS analysis was performed immediately and then 48 hours later. The results were compared to each other.

The optical properties of the GNP@ICG were recorded in the wavelength range of 300–1000 nm using UV-visible spectroscopy (UV 1700, Shimadzu Corp, Japan). The morphology of the GNP@ICG was determined using a scanning electron microscope (FE-SEM LMU TESCAN BRNO-Mira3, Czech Republic), operating at an acceleration voltage of 26 kV. TEM (Gatan model 791, Philips CM 12, Poland) was carried out to evaluate the morphology and size distribution of the GNPs. Infrared spectra were recorded with an FTIR spectrometer (AVATAR 370, Thermo Nicolet AVATAR 370 FTIR, USA) to investigate possible chemical interactions between ICG and GNP@ICG. X-ray diffraction (XRD) analysis (Bruker 9XS; G8ADVANCE, Germany) was performed to identify the crystallographic structure of GNP. Measurements were performed at voltage 40 kV and current 30 mA over the 2θ range of 20° to 80°.

Cell studies

Cell culture

DFW (human melanoma cell line, C496) and HFF (normal human foreskin fibroblast cell line, C163) were purchased from Pasteur Institute in Iran. DFW was cultured in RPMI-1640, and HFF was cultured in DMEM. All media were supplemented with 10% FBS and 0.5% penicillin-streptomycin. The cells were kept in a humidified incubator with a temperature of 37˚C and 5% CO_2. They were separated for passage using 0.25% trypsin-EDTA.

Cytotoxicity

To assess the toxicity of GNP@ICG on DFW and HFF cell lines, they were seeded in 96-well plates at densities of 10,000 and 7,000 cells/well, respectively, and incubated at 37˚C and 5% CO_2 for one day. The cells were probed for 24 hours at various concentrations (0-80 mg/L) of GNP@ICG added to the medium. Subsequently, to remove extra nanoparticles, the cells were rinsed with phosphate buffered saline (PBS) three times. Finally, the cell viability was analyzed by MTT assay after 24 hours.

Experimental treatments

The plasma device used in this study is a plasma jet (Satia knowledge based company; Semnan, Iran) consisting of two electrodes, A carbon center electrode connected to a high voltage power supply and a copper ground electrode attached to the ground. In this study, a high voltage power with a frequency of 13 kHz and a peak-to-peak voltage of 5 kV was given to the electrodes. Pure helium gas (99.999%) was also used to generate the plasma at a flow rate of 4-5 L/minutes. The length range of the plasma flame was set to 35-45 mm and the distance between the nozzle tip and the bottom plate was set to 25 mm. The gas temperature of the plasma jet was measured at 350 K. The biomedical application of CAP is primarily based on its ability to produce and form effective amounts of reactive species. Emission spectroscopy (OES) was used to confirm the presence of these species and their derivatives.

The cells were radiated with 8 MeV electron irradiation (linear accelerator Elekta Precise model, Germany) at a dose rate of 2 Gy/minutes with distance of 100 cm from the X-ray tube and gantry at 180 degrees position. Field dimensions were adjusted by using a 20*20 cm applicator and Perspex plates were used to set the build-up before the cells (15 mm thickness under the plate) as well as to remove the scatters from the plate (20 mm thickness on the plate). RT was performed at 1, 2, and 4 Gy.

Treatment groups consist of the following without and with 20 mg/L GNP@ICG (based on the cytotoxicity of GNP@ICG) for both cell lines: the control group (C), the plasma treatment groups (CAP and GNP@ICG+CAP), the radiotherapy groups (RT and GNP@ICG+RT), and the combined radiotherapy and plasma therapy groups (GNP@ICG+CAP+RT at various intervals 0 and 24 hours).

For all treatment groups, DFW and HFF cells were first seeded on 96 well plates and incubated overnight. Next, GNP@ICG (20 mg/L GNP@ICG containing 16 mg/L ICG and 20 mg/L GNP) was added to the cells. At the end of the incubation period, the cell plates were rinsed twice with PBS and replaced with a fresh medium. Afterward, in plasma treatment groups, the cell plates were treated with CAP at room temperature for different times (0, 15, 30, 60, and 90 seconds). In radiation therapy, cells irradiated with 8 MeV electron at various doses of 1, 2, and 4 Gy. To assess the efficacy of combined RT with CAP, the cells were first treated with CAP for 30 and 60 seconds, then irradiated with 2 Gy dose of radiation immediately and after 24 hours.

Evaluation of treatments

MTT assay

The MTT assay was used to identify the cytotoxicity of GNP@ICG and the effects of plasma and radiation therapy to find optimal concentrations of GNP@ICG and appropriate doses of RT and CAP, respectively. In this regard, the cells were assessed 24 hours after the end of treatments. Briefly, 100 µl of FBS-free medium

and 10 µl of MTT reagent (5 mg/mL in PBS) were added to all wells and incubated for 4 hours in the darkness. This test is based on the measurement of cell viability in terms of reducing activity as an enzymatic conversion of the tetrazolium to water-insoluble formazan crystals by dehydrogenase activity generated in the mitochondria of living cells. After that, the medium was removed and then for dissolving the formazan crystals, 200 µl of DMSO replaced. At the end, plates were shaken in the dark for 10 minutes. An ELIZA reader was used to measure the absorbance of the formazan solution at a wavelength of 570 nm as opposed to the reference wavelength of 630 nm. Finally, the relative cell viability rate was calculated by the absorbance ratio of the treatment group to the control group. All examinations were repeated more than three times.

Flow cytometry

To measure apoptosis and necrosis of cells treated with RT and CAP using the Annexin V-FITC/ PI flow cytometry kit, firstly, the cells were treated, incubated for 24 hours, rinsed with PBS, separated with trypsin, centrifuged at 1500 rpm for 5 minutes, then combined with the binding buffer. FITC-labeled Annexin V (2 µl) and PI (2 µl) were added to and pooled in 500 µl cell suspension. After 15 minutes of incubation in the dark, apoptosis/necrosis analysis was performed by flow cytometry (BD FACSCalibur, USA), and the data were analyzed by FlowJo software (version 7.6.1).

Colony formation assay

The colony formation assay (CFA) was accomplished to assess the ability of cells to develop as colonies after treatment. The cells were seeded in 6-well plates at a density of 600, 800, 1000, and 1200 cells/well for the control group, and a radiation dose of 1, 2, and 4 Gy. Following cell adhesion, they were treated in various groups according to the method described above. The groups contained control, GNP@ICG+RT, and GNP@ICG+CAP (60 seconds)+RT at 0 and 24 hours intervals. Then, colonies were allowed to form after 10 days of incubation. Finally, colonies were rinsed, fixed and stained with PBS, methanol, and Giemsa, respectively. It was calculated only colonies including more than 50 cells. The surviving fraction (SF) of each group was normalized to the plating efficiency (PE) associated to the control group. The SF was calculated by the below formula (26):

Plate efficiency (PE) = (number of colonies in the control group)/ (number of cultured cells)

Cell survival fraction = (number of colonies in the experimental group) / (number of cells in the experimental group × PE)

Synergistic index

We have defined a synergistic index (Syn) to determine if synergistic or additive effects have occurred in cell death (CD) caused by combined therapy including GNP@ICG+CAP+RT compared to CD of either treatment alone without interval (Syn.1) and 24 hours intervals (Syn.2) on melanoma and fibroblast cells.

$$Syn(1) = (CD(CAP + GNP@ICG + RT(2Gy))\ 0\ h) / (CD(CAP) + CD(GNP@ICG) + RT(2Gy))$$

$$Syn(2) = (CD(CAP + GNP@ICG + RT(2Gy))\ 24\ h) / (CD(CAP) + CD(GNP@ICG) + RT(2Gy))$$

Statistical analysis

The results were completed by repeating the tests three times and stated as mean values ± standard deviation (SD). The Kolmogorov-Smirnov nonparametric test was used to assess the normality of the data. We ran a one-way ANOVA followed by Tukey's tests to compare the mean differences. P-values below 0.05 were regarded as statistically significant.

Results

Characterization of synthetic nanoparticles

The size distribution of GNP and GNP@ICG were measured by DLS analysis. The hydrodynamic diameter of GNP and GNP@ICG is 24.3 and 31.5 nm, respectively. The Zeta potential of GNP and GNP@ICG were -1.5 and -7.8 mV, which was engaged to validate the excellent reaction. According to the results, the zeta potential of GNP@ICG is higher negative than GNPs. This finding is that the SO_3^- group in the ICG induces a negative charge on the surface of NPs. By comparing the hydrodynamic size of the NPs based on the DLS results, it was observed that the size of the nanoparticles did not change after 48 hours, indicating good stability of the nanoparticles (Fig.S1, See Supplementary Online Information at www.celljournal.org).

Figure 1A shows the UV-Vis spectra of GNP, ICG, and GNP@ICG. UV-Vis spectrometry was employed to characterize the synthesized conjugated NPs. It is clear that the spectrum of the GNP shows the dispersion of GNP. The absorption spectrum of ICG shows strong absorption in 700-780 nm depending on the ICG concentration. GNP shows characteristic surface absorption at 520 nm, confirming that the GNP are spherical. In addition, GNP@ICG shows peaks at 520, 709, and 778 nm, indicating the presence of GNP and ICG in the conjugated nanoparticles. For surface analysis of the synthesized nanoparticles and compared with free ICG, the FT-IR spectra were obtained from dried GNP@ICG and ICG (Fig.1B). According to FT-IR spectra of ICG, the absorption bands around 3430 cm^{-1}, 1400 cm^{-1}, 1090 cm^{-1}, and 891 cm^{-1} can be assigned to O-H stretching vibration, SO_3H and C=C bond, sulfoxide, and C-H ring bending vibration, respectively, exhibiting the characteristic peaks of ICG. According to GNP@ICG, the characteristic peak at 1410 and 1590 cm^{-1} correspond to the symmetric and anti-symmetric stretching of COO– related to citrate ion. These data confirm the interaction between citrate ions and GNP. In addition, the existence of absorption peaks of ICG (3430, 1400, 1090, and 891 cm^{-1}) in the IR spectrum of GNP@ICG can confirm that ICG was successfully conjugated on the GNP surface.

SEM images of GNP and GNP@ICG and their size distribution histogram obtained by ImageJ software are shown in Figure 1C-F. It can be observed that the nanoparticles are spherical shape with average diameters of 19.49 and 24 nm, respectively. Also, as shown in Figure 1G. The spherical structure of GNP can be observed clearly in the TEM image. The shape and mean diameter of GNP evaluated by TEM imaging (around 20 nm) were correlated to FE-SEM and DLS measurements. The XRD pattern of GNP is shown in Figure 1H. Crystalline nanoparticles structure specified through four peaks corresponding to standard Bragg reflections (111), (200), (220), and (311) of face centers cubic lattice. The intense peak at 38, 44.3, 64.5, and 77.7 nm determines preferential growth in the (111, 200, 220, and 311) direction.
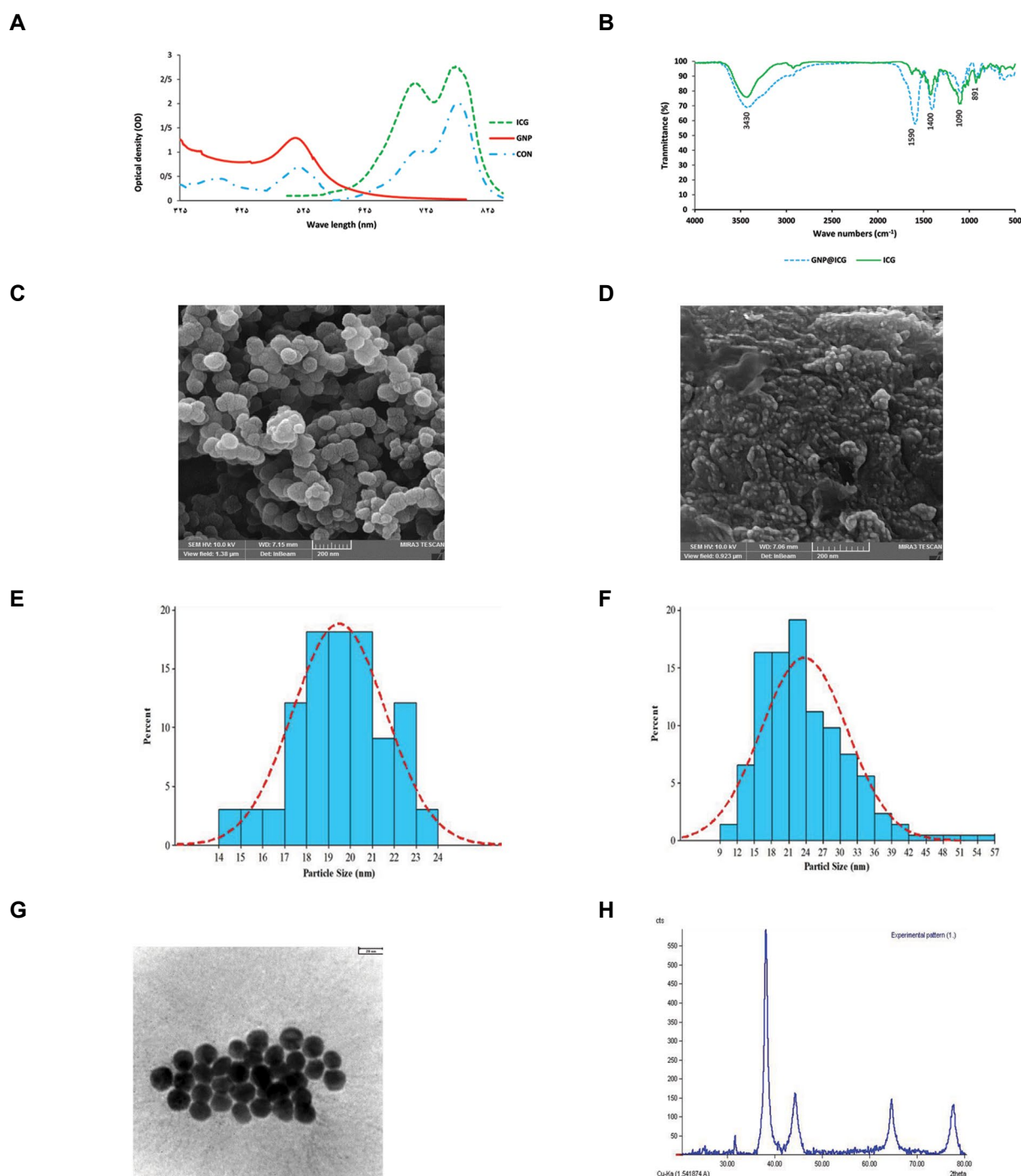
A

B

C

D

E

F

G

H

Fig.1: The specifications of synthesized nanoparticles. **A.** The UV-visible spectrum of GNP (20 mg/L), ICG (16 mg/L) and GNP@ICG (20 mg/L based on the concentration of GNP), **B.** The FT-IR spectra of GNP@ICG (20 mg/L based on the concentration of GNP) and free ICG (16 mg/L), **C.** Field Emission Scanning Electron Microscopy (FE-SEM) images of GNP (scale bar: 200 nm), **D.** FE-SEM images of GNP@ICG (scale bar: 200 nm), **E.** Hydrodynamic size distribution of GNP, **F.** Hydrodynamic size distribution of GNP@ICG, **G.** TEM image of the gold nanoparticle (scale bar: 20 nm), and **H.** XRD analysis of gold nanoparticles. GNP; Gold Nanoparticles, ICG; Indocyanine green, FT-IR; Fourier transform infrared spectroscopy, TEM; Transmission electron microscopy, and XRD; X-Ray diffraction analysis.

Spectroscopy analysis

The emission spectrum of CAP was obtained by spectroscopic analysis (Fig.2A). Figure 2B displays a schematic illustration of the CAP device used in this experiment. As shown in Figures 1A and 3, the absorption spectrum of the ICG is superimposed on the emission spectrum of the CAP. The most prominent emission peaks for CAP include 320, 330, 350, 391, 400, 460, and 707 nm. As one can see, the absorption peak of ICG at wavelengths 710 to 780 corresponds to the emission spectrum of the He-CAP.
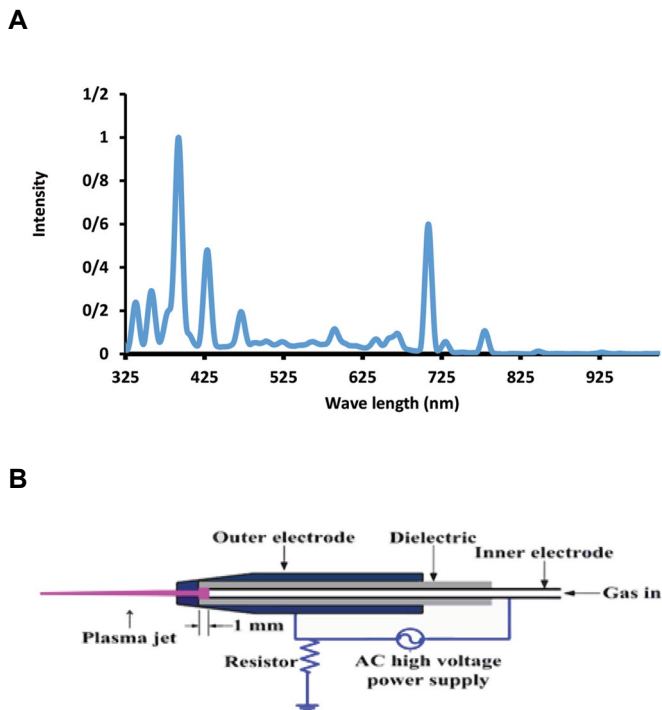
A

B

Fig.2: The characterization of CAP. **A.** The emission spectrum of CAP-He and **B.** Schematic illustration of the plasma jet. CAP-He; Cold Atmospheric helium plasma and AC; Alternating current.

MTT assay

To select an optimal concentration of GNP@ICG NPs and evaluate CAP treatment and radiation therapy, the MTT assay was carried out to measure the metabolic viability of DFW (cancer cells) and HFF (normal cells) in different treatment groups. After incubating cells with varied concentrations of GNP@ICG (0-80 mg/L) for 24 hours, it was shown that concentrations of GNP@ICG less than 20 mg/L had only a slight effect on both cells. It was concluded that 80 mg/L was the most toxic and killed nearly 51% and 72% of the melanoma and fibroblast populations, respectively (Fig.3A). The low toxic concentration of GNP@ICG (20 mg/L of GNP@ICG containing 16 mg/L ICG and 20 mg/L GNP) was used to evaluate the inhibition of cells proliferation in RT, CAP, and combined therapy groups. Treatments were performed as described in Material and Methods.

The RT results (Fig.3B) shows the radiation resistance of melanoma cells. Moreover, in both cells a significant difference was observed between RT and GNP@ICG+RT groups (P<0.05), which indicates the role of GNP@ICG as a radio-sensitizer.

Figure 3C shows the cell viability of DFW melanoma cells at different times of plasma irradiation as well as incubation with GNP@ICG. However, cell survival at 15 seconds treatment with CAP had no effect on cells, with increasing plasma irradiation time, cell survival percentage decreased significantly, so that in the 90-second group in the presence of GNP@ICG, the survival percentage reached 14% (P<0.01). Also, cell survival in plasma therapy with GNP@ICG was significantly reduced compared to the drug-free group, which can confirm the GNP@ICG optical sensitivity in PDT with CAP. In order to determine whether plasma therapy is selective for cancer cell lines, HFF cells were treated under similar conditions. The results showed that increasing the plasma time had no effect on the survival of HFF cells. The results were the same even in the treatment group that received GNP@ICG.

Based on these findings, doses of 30 and 60 seconds for CAP therapy and 2 Gy for RT were selected for irradiation in subsequent experiments. Synergistic enhancement was observed in DFW cells treated with combination therapy in a dose-dependent manner compared to either the control group or each modality alone. This means that pre-treated with CAP before RT promoted radiation effects on tumor cell death and amplified influence at higher doses. In contrast, no significant difference was measured between these groups for the HFF cell line (P>0.05). It is worth noting that plasma plays a crucial part in combining radiation therapy with CAP for a selective and effective therapy.

To evaluate the effect of interval in combined therapy, cells were exposed to RT immediately and 24 hours following CAP therapy. It was found that administration of RT 24 hours after CAP therapy can induce more cell death in DFW cells than the employment of these modalities immediately, whereas this discrepancy was not observed in HFF cells (Fig.3D).

Flow cytometry

Flow cytometric assays were used to evaluate the induction of apoptosis and necrosis in various treatments of melanoma and fibroblast cell lines. The degree of apoptosis induction was quantified by Annexin V-FITC/PI staining. The flow cytometry experiment indicated a distribution pattern of cells treated with GNP@ICG, CAP, and RT alone and in combination treatment (GNP@ICG+CAP+RT) in sequences of 0 and 24 hours in Figure 4. As seen in Figure 4A, in melanoma cells, the percentage of apoptosis in combination RT with GNP@ICG was not significantly different from RT alone. While this difference made a significant difference in the treatment of CAP with GNP@ICG. In addition, the apoptosis rate was measured the highest amount in the combinatorial treatment group (GNP@ICG+RT+CAP), and it was established that the intervals between treatments did not induce apoptosis (P<0.05). We also evaluated the therapeutic effect on fibroblast (HFF) cell lines (Fig.4C). HFF cells were treated similarly to melanoma treatment. It was shown that RT, CAP, or combined CAP with RT did not induce significant apoptosis in fibroblast cells (P>0.05).
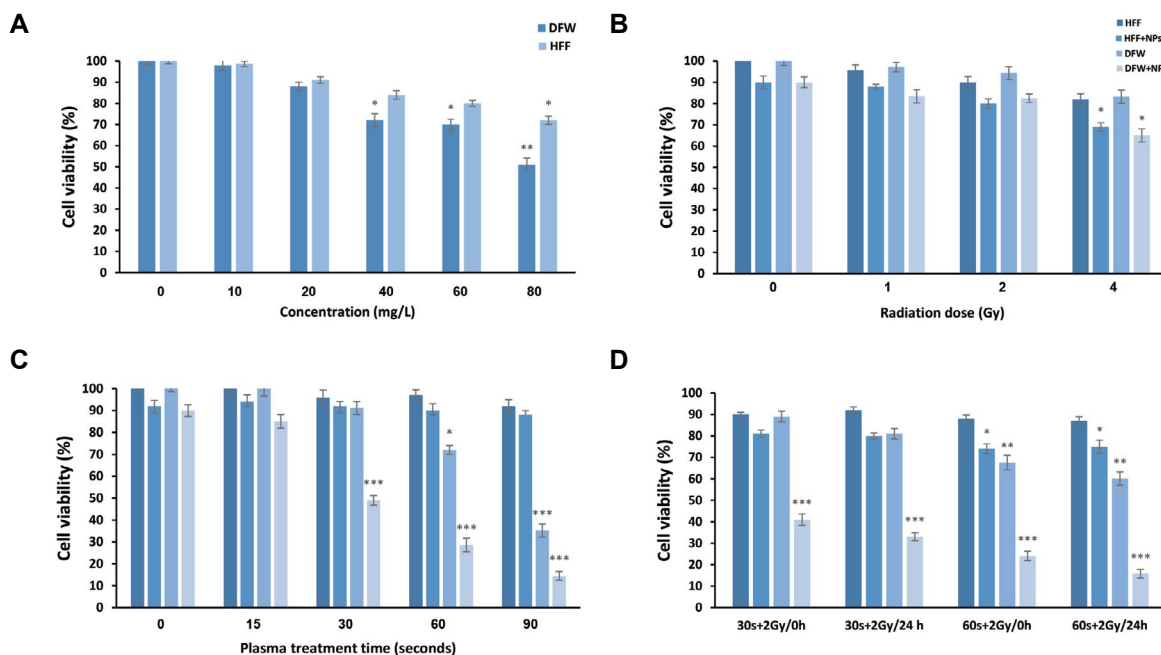
Fig.3: MTT assay results on melanoma (DFW) and fibroblast (HFF) cell lines at 24 hours. **A.** The survival rate of DFW and HFF cells incubated with different concentrations of GNP@ICG in 24 hours. The concentration of 10 μM which caused 10% cell death was selected for following treatments. **B.** The survival percentage of cells treated with radiotherapy. **C.** The survival percentage of cells treated with CAP. **D.** The viability of the cells treated to 2 Gy RT following NPs and CAP (30 and 60 seconds) immediately and 24 hours later. Data are shown as the mean ± SD (n=3). A comparison of the difference between each group and the control group was presented as *; P<0.05, **; P<0.01, and ***; P<0.001. CAP; Cold atmospheric plasma, NPs; GNP@ICG, RT; Radiotherapy, 30s+2Gy/0h; Combined therapy 30-seconds CAP and 2 Gy radiation immediately, 30s+2Gy/24h; Ccombined therapy 30-seconds CAP and 2 Gy radiation with 24 hours interval, 60 s+2Gy/0h; Combined therapy 60-seconds CAP and 2 Gy radiation immediately, and 60s+2Gy/24h; Combined therapy 60-seconds CAP and 2 Gy radiation with 24 hours interval.
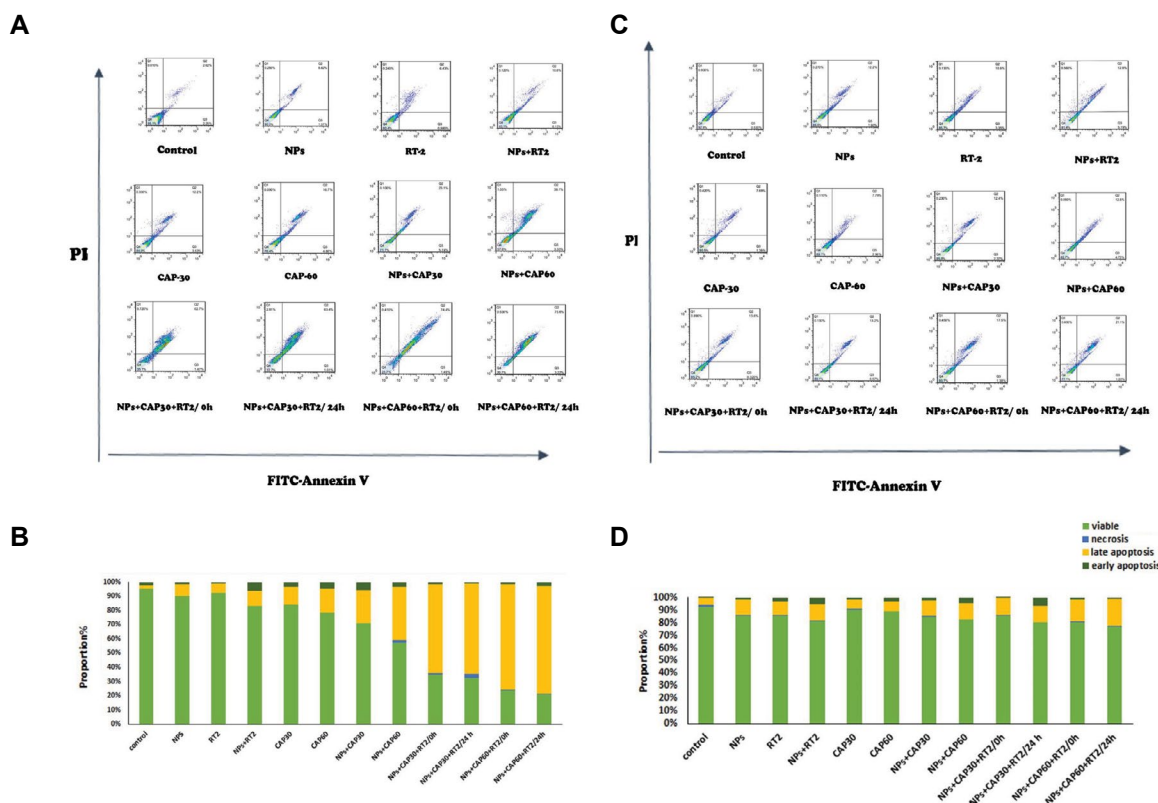

Fig.4: Flow cytometry results of DFW and HFF cell lines. **A.** The Annexin-V-FITC assay for detecting the apoptosis and necrosis of DFW cells, **B.** The diagram of the percentage of apoptotic and necrotic of DFW cells after treatment with different groups, **C.** The Annexin-V-FITC assay for detecting the apoptosis and necrosis of HFF cells, and **D.** The diagram of percentage of apoptotic and necrotic of HFF cells in different groups. DFW; Melanoma cell line, HFF; Health foreskin fibroblast, CAP; Cold atmospheric plasma, NPs; GNP@ICG, RT; Radiotherapy, 30s+2Gy/0h; Combined therapy 30-seconds CAP and 2 Gy radiation immediately, 30s+2Gy/24h; Ccombined therapy 30-seconds CAP and 2 Gy radiation with 24 hours interval, 60 s+2Gy/0h; Combined therapy 60-seconds CAP and 2 Gy radiation immediately, and 60s+2Gy/24h; Combined therapy 60-seconds CAP and 2 Gy radiation with 24 hours interval.

Colony formation assay

CFA was used to measure the ability of cells to maintain reproductive integrity over a long time after various treatments. CFA is the gold standard to identify reproductive cell death after ionizing radiation therapy. Figure 5 shows the effects of GNP@ICG and CAP (60 seconds) in different intervals and radiation doses on DFW melanoma cell lines in monolayer cultures. As can be concluded from the results, GNP@ICG alone had no significant effect on cell colonization compared to the control group (P>0.05). In the associated combined therapy, the reduction in SF was considerably more significant than in the control group receiving RT alone (P<0.05), which confirmed that CAP and GNP@ICG reduced radiation-induced clonogenic melanoma cell death in a dose-dependent manner. As can be seen in Figure 5A, in the combined treatment, the number of colonies and their size has decreased with increasing radiation dose, which indicates a decrease in the ability of cells to form colonies. The considerable difference between the combined treatment and control groups demonstrated that CAP plays a function in cancer cell synergy and radio-sensitivity. Furthermore, while combination treatment had the lowest cell viability, the gap between them did not produce significant effects, confirming the findings of the apoptosis experiment.

Synergistic index

The values of synergism index for combine therapy GNP@ICG+CAP+RT at 0 and 24 h intervals on melanoma and fibroblast cells were calculated in accordance with Formula. The synergistic indices were calculated more than 1 on melanoma cells (2.18 ± 0.02 and 1.65 ± 0.02 for 30 and 60 seconds, respectively treatment with CAP and 2 Gy radiotherapy immediately, and also 2.48 ± 0.03 and 1.82 ± 0.02 for 2 Gy radiotherapy following 30 and 60 seconds, respectively plasma treatment after 24 hours) which shows proposed treatment approaches had the synergistic effects. However, the synergistic index was calculated lower than 1 in all treatment groups on fibroblast cells.
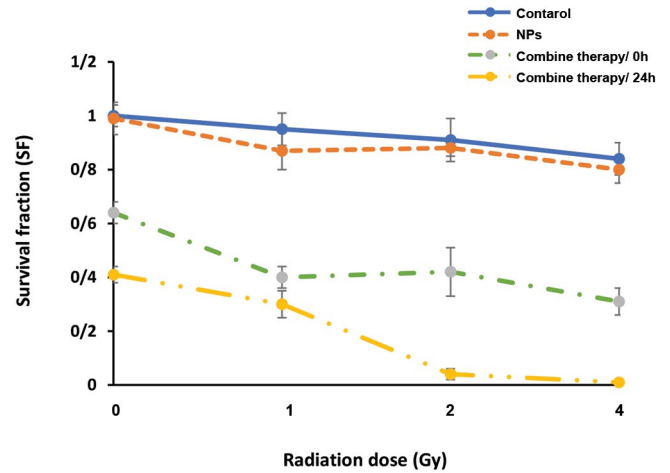
A
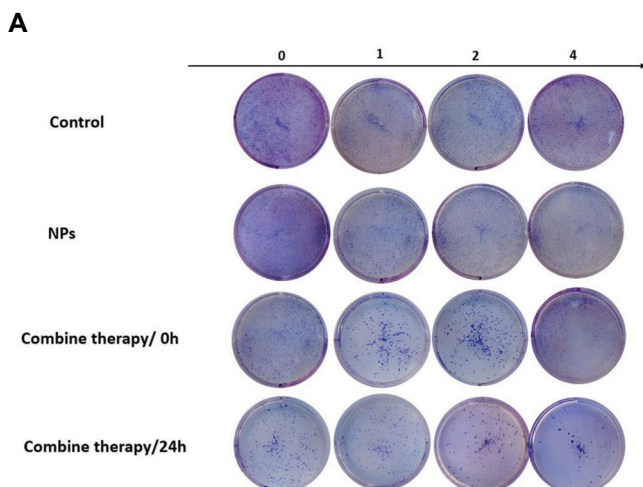
B

Fig.5: The treatment results via colony assay for DFW cells. **A.** The representative colony formation images of DFW cells in different treatments. **B.** Clonogenic cell survival curves. The surviving fraction in the colony-forming assay was calculated and normalized to that of the unirradiated control cells. Data were obtained from three independent experiments (mean ± SD, n=3). NPs; Gold nanoparticle conjugated with Indocyanine green, Combine therapy/0 hour; Treatment with 2 Gy radiotherapy immediately after 60 seconds cold plasma therapy, and Combine therapy/24 hours: treatment with 2 Gy radiotherapy 24 hours after 60 seconds cold plasma therapy.

Discussion

Melanoma accounts for just around 1% of all skin malignancies, yet it is responsible for the majority of mortality (1). Melanoma is difficult to treat because to its aggressive nature, resistance to established cancer therapies such as radiation therapy and chemotherapy, and poor response (2). Therefore, a new antitumor strategy is needed in this area. We have proposed an effective strategy for the DFW cell line derived from skin cancer to improve its radiation sensitivity and treatment efficiency.

CAP is a pioneering approach in cancer therapy. CAP contains different elements such as electrons, free radicals, charged particles, UV photons, and various excited molecules. The existence of different ingredients in plasma composition resulted in unique properties. For example, CAP is a potent generator of reactive oxygen species (ROS), which may be exploited to sensitize hypoxic malignancies to therapies (27). During plasma treatment, plasma introduces ROS into cells, disrupting oxidative equilibrium. By activating intracellular signaling pathways, excessive oxidative stress might lead to cell death (28). Moreover, CAP has several peaks in the emission spectra, so it is possible to use types of photosensitizers in CAP therapy. In addition, the difference between the cell membrane electric field and the CAP-induced transient electric field opens channels and increases the number of nanoparticles absorbed, resulting in improving processing efficiency (16).

Nanoparticles are being used in cancer treatment to take a more tailored approach. We created a novel conjugation that may be employed as a photo-radio-sensitizer to

improve treatment efficiency in this investigation. GNP have risen to the top of the list of metal nanoparticles used in bioanalytical studies. In this respect, gold nanospheres were successfully synthesized and conjugated with ICG as a photosensitizer. The results of photophysical properties analysis further confirmed that ICG could be conjugated by GNP. The existence of the characteristic absorption peak of ICG in the IR spectrum of GNP@ICG can confirm that ICG was successfully conjugated on the GNP surface. The size of GNP@ICG measured by DLS, TEM, and SEM was approximately 20 nm. Size 10-100 nm for GNP@ICG has been approved that is a suitable size to easily enter cells and increase uptake. The zeta potential calculated a good negative charge and confirmed the stability of GNP@ICG.

Due to the fact that RT for melanoma patients is performed with electrons as well as the advantages of electrons over photons (29) in this superficial tumor, we used electrons instead of photons in this study. MTT assay measured a considerable decrease in viability in treatment with radiation and GNP@ICG (20 mg/L). Since several studies have reported the radiosensitizing effect of GNP (30, 31) and Sazgarnia et al. (32) showed a low radiosensitizing effect of ICG, it is understood that the decrease in the cell viability measured is in terms of GNP in treatment.

In CAP therapy, according to the cell survival results after different treatment time, it can be found that plasma causes a notable inhibitory effect on DFW cells. The enhanced treatment efficacy by CAP was significantly improved in the presence of GNP@ICG, possibly in terms of the more absorption of GNP@ICG into cells following treatment with plasma. Our findings are in agreement with Zhu' research (4) observed that the combination of fluorouracil-loaded PLGA nanoparticles and CAP has enhanced efficacy for solid tumors treatment that inhibits synergistically cancer cell growth when compared individually. They also found that CAP promotes nanoparticle absorption while also lowering MMP2, MMP9, MTDH, and VEGF gene expression, all of which are linked to metastasis. Another explanation for plasma therapy's great effectiveness might be the photodynamic impact caused by ICG. Several studies have used different photosensitizers in CAP and evaluated the photodynamic effects of CAP on a variety of tumors. Karami used 5-ALA as a photosensitizer and observed the synergistic effect of CAP (33) and Wang et al. (34) treated melanoma cells with protoporphyrin IX and CAP. In a similar study, Vejdani Noghreiyan et al. (35) evaluated the PDT effects of CAP on ICG and PpIX at various concentrations (5-50 μM). The cells (HT-29 and MCF-7) were treated with CAP in 1 and 2 minutes irradiation. Results showed increased effectiveness of plasma treatment in the presence of ICG and PPIX. Furthermore, this effect was found to be cell line dependent.

The superiority of CAP over other treatment modalities is the ability of plasma to kill cancer cells selectively, while its effect on healthy cells is negligible. To evaluate the selectivity effect in CAP therapy, HFF cells were treated in conditions similar to DFW cells. Comparing the viability of the two cell lines showed that DFW cells were substantially more susceptible to plasma than HFF cells. Various studies have shown the selectivity of CAP treatment (14, 36). Lin et al. (37) evaluated the plasma inhibitory effects in different tumor cells (A549 and HeLa) and normal cells (HepG2 and GM0637) *in vitro* and *in vivo*. They observed that plasma exerted a more proliferation inhibitory effect on tumor cells than normal cells. Biscop et al. (38) proposed a hypothesis that the reason for CAP selectivity could be influenced not only by the tumor or normal condition, but also by the culture medium and cell type. In this regard, they examined different cancer cells (A549, Mame-3M, A375, and, and U87) with their non-cancer counterparts (HEMa, HA, and BEAS-2B) and other culture mediums (DCBM, RPMI1640, DMEM, BEGM, and AM). They found that plasma has caused a selectivity effect between tumor and normal cells, and cell culture and cell type have less impact on the results.

Various features of a standardized treatment approach should be reviewed and chosen based on the general characteristics of CAP attributes for the clinical application of combined CAP and RT. Although some research have looked at the efficacy of plasma in conjunction with other treatment such as hyperthermia (39), chemotherapy (40), and PDT, no studies have looked at the combination of radiation therapy with CAP plus multifunctional nanoparticles. Currently, photocytotoxic damage is known to be caused by singlet oxygen acting on the cell membrane, but nuclear DNA is the main target for cell killing by ionizing radiation. Since PDT and RT cause damage to different targets synergy between them to kill the cells may improve tumor control. Considering these findings, it seems particularly interesting to assess the antitumor effects of innovative combination treatments. Reducing the dose of ionizing radiation while maintaining the desired tumor suppressor effect is important because it minimizes the potential damage caused by RT to normal problems. We found that the combination therapy (GNP@ICG+CAP+RT) induces an important cytotoxic effects on the melanoma cell lines. Since such effects could not be induced by high-dose radiation or using GNP@ICG, it was proved that CAP caused a synergistic improvement in combination therapy. It is accordance with Lin study (37). Similar to our study, they used CAP (based on Ar/O2 gas) 24 hours after RT to increase radiosensitivity in the treatment of various types of cancer, and compared the results to the treatment results of healthy cells. It was founded CAP inhibits the growth of tumors and induces apoptosis. Moreover, the effect of CAP on cancer cells is more effective than on normal cells. ROS generation is the reason why combination therapy has a synergistic effect.

Apoptosis, or programmed cell death, determines a genetically encoded cell death program that is

biochemically and morphologically completely different from accidental or necrotic cell death. The flow cytometric assay was broadly used to assess apoptosis in a variety of experimental methods. It is based on the principle that apoptotic cells are characterized by DNA fragmentation and the absence of nuclear DNA content, among other normal properties. Using fluorescent dyes such as FITC and PI that can bind and label DNA, a flow cytometry analysis can quickly and accurately measure the DNA content of cells. The induction of apoptosis by DNA damage or lipid peroxidation of the cell membrane is the most significant mechanism of the cell-plasma interaction, thus a flow cytometry assay to determine the amount of impact is a good test. Besides, apoptosis was identified as an attractive cell death pathway in response to cancer treatment modalities compared to necrotic cell death in terms of the damage to adjacent healthy cells.

Flow cytometric results show that under RT and CAP irradiation, the majority of cell death in melanoma and fibroblast cells is caused by apoptosis, and significant levels of apoptosis occur, especially in the combination treatment group (GNP@ICG+CAP+RT). It showed that it did about 75% in the DFW cells with combined therapy. However, the number of necrotic cells was measured insignificant. The flow cytometric results confirmed the MTT results. Our results are in agreement with previous results, as CAP promoted unparalleled levels of apoptosis induction in cancer cells (40).

The minimum survival in cancer cells was attained when radiation therapy was given 24 hours after CAP therapy in the presence of GNP@ICG. Cell cycle arrest was proposed as a potentially effective technique for inhibiting cancer cell growth. As a result, cell cycle modulation is a mechanism that may improve RT sensitivity during CAP therapy. There hasn't been any research on the appropriate sequence and interval between CAP and RT for maximum therapeutic effectiveness. It might go better in as little as 24 hours or as long as a week.

The colony assay is the gold standard test for measuring cellular death induced by ionizing radiation. It was performed to evaluate the long-term effects of RT and combined therapy on the DFW cell line. The results of the colony test showed a very low curve slope for the control group, which confirms the radiation resistance of melanoma cells. It was found that GNP@ICG had no effect on colony formation, according GNP@ICG+CAP+RT), especially for the 24 hours interval, increased slope indicates a decrease in the number of colonies, thusly the effectiveness of combination therapy on radiation-resistant melanoma cells. Better results require more complementary *in vitro* and *in vivo* studies on various cancer and normal cell lines, and it needs to evaluate other physical parameters such as the voltage, gas and other CAP techniques.

Conclusion

Using non-ionizing cold plasma treatment along with RT reduces the side effects of ionizing radiation, such as secondary cancer risks and damage to sensitive tissues adjacent to the tumor, and improves treatment outcomes. The present study involved the combination of plasma treatment and RT in the presence of GNP@ICG, as a photo-radio sensitizer, on DFW and HFF cell lines. It was found that plasma alone or in combination with radiotherapy is able to reduce the survival of melanoma cells without significantly damaging healthy ones. Though plasma is a nascent technique and requires further *in vivo* and preclinical studies, multiple studies, including this one, confirm that it serves as an adjunctive therapy. The incidence of PDT with CAP was also reaffirmed. To our knowledge, it is also the first time we have seen proof that GNP@ICG has been proven effective in collaboration with plasma and radiation therapy. Furthermore, a 24 hours interval between the plasma and radiation remedies improves treatment results.

Acknowledgements

Authors' Contributions

S.M.; Participated in study design, data collection, drafting and statistical analysis. A.Sh., A.S.; Were responsible for overall supervision, data evaluation, and contributed to conception and design. N.A., S.A.A.; Contributed extensively in interpretation of the data and the conclusion. All authors read and approved the final manuscript.

References

1. Jenkins RW, Fisher DE. Treatment of advanced melanoma in 2020 and beyond. J Invest Dermatol. 2021; 141(1): 23-31.
2. Trappetti V, Fazzari JM, Fernandez-palomo C, Scheidegger M, Volarevic V, Martin OA, et al. Microbeam radiotherapy—a novel therapeutic approach to overcome radioresistance and enhance anti-tumour response in melanoma. Int J Mol Sci. 2021; 22(14): 7755.
3. Zhang L, Ji Z, Zhang J, Yang S. Photodynamic therapy enhances skin cancer chemotherapy effects through autophagy regulation. Photodiagnosis Photodyn Ther. 2019; 28: 159-165.
4. Zhu W, Lee SJ, Castro NJ, Yan D, Keidar M, Zhang LG. Synergistic effect of cold atmospheric plasma and drug loaded core-shell nanoparticles on inhibiting breast cancer cell growth. Sci Rep. 2016; 6: 21974.
5. Correia JH, Rodrigues JA, Pimenta S, Dong T, Yang Z. Photodynamic therapy review: principles, photosensitizers, applications, and future directions. Pharmaceutics. 2021; 13(9): 1332.
6. Li XY, Tan LC, Dong LW, Zhang WQ, Shen XX, Lu X, et al. Susceptibility and resistance mechanisms during photodynamic therapy of melanoma. Front Oncol. 2020; 10: 597.
7. Nakajima K, Ogawa M. Phototoxicity in near-infrared photoimmunotherapy is influenced by the subcellular localization of antibody-IR700. Photodiagnosis Photodyn Ther. 2020; 31: 101926.
8. Babington P, Rajjoub K, Canady J, Siu A, Keidar M, Sherman JH. Use of cold atmospheric plasma in the treatment of cancer. Biointerphases. 2017; 10(2): 029403.
9. Mohd Nasir N, Lee BK, Yap SS, Thong KL, Yap SL. Cold plasma inactivation of chronic wound bacteria. Arch Biochem Biophys. 2016; 605: 76-85.
10. Kleineidam B, Nokhbehsaim M, Deschner J, Wahl G. Effect of cold

plasma on periodontal wound healing—an in vitro study. Clin Oral Investig. 2019; 23: 1941-1950.

11. Keping YA, Qikang JI, Zheng C, Guanlei DE, Shengyong YI, Zhen LI. Pulsed cold plasma-induced blood coagulation and its pilot application in stanching bleeding during rat hepatectomy. Plasma Sci Technol. 2018; 20(4): 044005.

12. Mateu-Sanz M, Tornín J, Brulin B, Khlyustova A, Ginebra MP, Layrolle P, et al. Cold plasma-treated ringer's saline: a weapon to target osteosarcoma. Cancers (Basel). 2020; 12(1): 227.

13. Mirpour S, Piroozmand S, Soleimani N, Jalali Faharani N, Ghomi H, Fotovat Eskandari H, et al. Utilizing the micron sized non-thermal atmospheric pressure plasma inside the animal body for the tumor treatment application. Sci Rep. 2016; 6(1): 29048.

14. Yazdani Z, Mehrabanjoubani P, Biparva P, Rafiei A. Cytotoxicity effect of cold atmospheric plasma on melanoma (B16-f10), breast (mcf-7) and lung (a549) cancer cell lines compared with normal cells. J Mazandaran Univ Med Sci. 2020; 30(187): 38-48.

15. Sklias K, Santos Sousa J, Girard PM. Role of short- and long-lived reactive species on the selectivity and anti-cancer action of plasma treatment in vitro. Cancers (Basel). 2021; 13(4): 615.

16. Vijayarangan V, Delalande A, Dozias S, Pouvesle JM, Robert E, Pichon C. New insights on molecular internalization and drug delivery following plasma jet exposures. Int J Pharm. 2020; 589: 119874.

17. Bauer G, Graves DB. Mechanisms of selective antitumor action of cold atmospheric plasma-derived reactive oxygen and nitrogen species. Plasma Process Polym. 2016; 13: 1157-1178.

18. Mateu-Sanz M, Tornín J, Ginebra MP, Canal C. Cold atmospheric plasma: a new strategy based primarily on oxidative stress for osteosarcoma therapy. J Clin Med. 2021; 10(4): 893.

19. Kurita H, Haruta N, Uchihashi Y, Seto T, Takashima K. Strand breaks and chemical modification of intracellular DNA induced by cold atmospheric pressure plasma irradiation. PLoS One. 2020; 15(5): e0232724.

20. Hua D, Cai D, Ning M, Yu L, Zhang Z, Han P, et al. Cold atmospheric plasma selectively induces G0/G1 cell cycle arrest and apoptosis in AR-independent prostate cancer cells. J Cancer. 2021; 12(19): 5977-5986.

21. Fan J, Cheng Y, Sun M. Functionalized gold nanoparticles: synthesis, properties and biomedical applications. Chem Rec. 2020; 20(12): 1474-1504.

22. Aryal S, Bisht G. New paradigm for a targeted cancer therapeutic approach: a short review on potential synergy of gold nanoparticles and cold atmospheric plasma. Biomedicines. 2017; 5(3): 38.

23. Jawaid P, Rehman MU, Zhao QL, Misawa M, Ishikawa K, Hori M, et al. Small size gold nanoparticles enhance apoptosis-induced by cold atmospheric plasma via depletion of intracellular GSH and modification of oxidative stress. Cell Death Discov. 2020; 6: 83.

24. Chien YY, Wang TY, Liao PW, Wu WC, Chen CY. Folate-conjugaed and dual stimuli-responsive mixed micelles loading Indocyanine green for photothermal and photodynamic therapy. Macromol Biosci. 2018;18(6): e1700409.

25. Anshup A, Venkataraman JS, Subramaniam C, Kumar RR, Priya S, Kumar TR, et al. Growth of gold nanoparticles in human cells. Langmuir. 2005; 21(25): 11562-11567.

26. Hall EJ, Giaccia AJ. Radiobiology for the radiologist. 8th ed. Lippincottt William & Wilkins: 2018.

27. Szili EJ, Oh JS, Fukuhara H, Bhatia R, Gaur N, Nguyen CK, et al.

Modelling the helium plasma jet delivery of reactive species into a 3D cancer tumour. Plasma Sources Sci Technol. 2018; 27: 14001.

28. Farooq MA, Niazi AK, Akhtar J, Farooq M, Souri Z, Karimi N, Rengel Z. Acquiring control: The evolution of ROS-Induced oxidative stress and redox signaling pathways in plant stress responses. Plant Physiol Biochem. 2019; 141: 353-369.

29. Momeni S, Bahreyni Toosi MT, Anvari K, Gholamhosseinian H, Soleymanifard S. Comparing two radiotherapy techniques of whole central nervous system tumors, considering tumor and critical organs' dose provided by treatment planning system and direct measurement. J Cancer Res Ther. 2020; 16(6): 1470-1475.

30. Zhang Y, Huang F, Ren C, Liu J, Yang L, Chen S, et al. Enhanced radiosensitization by gold nanoparticles with acid-triggered aggregation in cancer radiotherapy. Adv Sci (Weinh). 2019; 6(8): 1801806.

31. Vlastou E, Diamantopoulos S, Efstathopoulos EP. Monte Carlo studies in Gold Nanoparticles enhanced radiotherapy: the impact of modelled parameters in dose enhancement. Phys Med. 2020; 80: 57-64.

32. Sazgarnia A, Bahreyni-Toosi MH, Montazerabadi AR, Ahmadi A. Indocyanine green acts as a photosensitizer but not a radiosensitizer: combined chemo-, photo-and radiotherapy of DFW human melanoma cells. J Exp Ther Oncol. 2016; 10(3): 189-196.

33. Karami-Gadallo L, Ghoranneviss M, Ataie-Fashtami L, Pouladian M, Sardari D. Enhancement of cancerous cells treatment by applying cold atmospheric plasma and photo dynamic therapy simultaneously. Clin Plasma Med. 2017; 7: 46-51.

34. Wang M, Geilich BM, Keidar M, Webster TJ. Killing malignant melanoma cells with protoporphyrin IX-loaded polymersome-mediated photodynamic therapy and cold atmospheric plasma. Int J Nanomedicine. 2017; 12: 4117-4127.

35. Vejdani Noghreiyan A, Imanparast A, Shayesteh Ara E, Soudmand S, Vejdani Noghreiyan V, Sazgarnia A. In-vitro investigation of cold atmospheric plasma induced photodynamic effect by Indocyanine green and Protoporphyrin IX. Photodiagnosis Photodyn Ther. 2020; 31: 101822.

36. Keidar M, Walk R, Shashurin A, Srinivasan P, Sandler A, Dasgupta S, et al. Cold plasma selectivity and the possibility of a paradigm shift in cancer therapy. Br J Cancer. 2016; 105(9): 1295-1301.

37. Lin L, Wang L, Liu Y, Xu C, Tu Y, Zhou J. Non-thermal plasma inhibits tumor growth and proliferation and enhances the sensitivity to radiation in vitro and in vivo. Oncol Rep. 2018; 40(6): 3405-3415.

38. Biscop E, Lin A, Van Boxem W, Van Loenhout J, De Backer J, Deben C, Dewilde S, Smits E, Bogaerts A. The influence of cell type and culture medium on determining cancer selectivity of cold atmospheric plasma treatment. Cancers (Basel). 2019; 11(9): 1287.

39. Moniruzzaman R, Rehman MU, Zhao QL, Jawaid P, Takeda K, Ishikawa K, et al. Cold atmospheric helium plasma causes synergistic enhancement in cell death with hyperthermia and an additive enhancement with radiation. Sci Rep. 2017; 7(1): 11659.

40. Saadati F, Mahdikia H, Abbaszadeh HA, Abdollahifar MA, Khoramgah MS, Shokri B. Comparison of direct and indirect cold atmospheric-pressure plasma methods in the B16F10 melanoma cancer cells treatment. Sci Rep. 2018; 8(1): 7689.